

Effect of strain on the electrical conduction in epitaxial films of $\text{La}_{0.7}\text{Ca}_{0.3}\text{MnO}_3$

Mandar Paranjape* and A. K. Raychaudhuri†

Department of Physics, Indian Institute of Science, Bangalore 560 012, India

N. D. Mathur and M. G. Blamire

Department of Materials Science and Metallurgy, Cambridge University, Cambridge CB2 3QZ, United Kingdom

We have used scanning tunneling microscopy and potentiometry to study the microstructure and nanoscopic current transport in thin films of $\text{La}_{0.7}\text{Ca}_{0.3}\text{MnO}_3$ grown on SrTiO_3 and NdGaO_3 substrates. Thin (50 nm) films, which are strained, show step-terrace growth, whereas relatively thicker film (200 nm), which is strain relaxed, shows well-connected grains. Charge transport in these films is inhomogeneous on the scale of nanometers. There are large variations in the local potential at grain boundaries as well as step edges. The value of the average field distribution at grain boundaries and step edges is found to be dependent on the strain in the film. Within the terraces local variations in potentials correlate with the nature of the strain in the film and this gives rise to inhomogeneous current flow in them.

Electronic transport in rare-earth manganites which show colossal magnetoresistance (CMR) has been a topic of much current interest.^{1,2} In these materials the resistivity (ρ) shows a peak at a temperature T_p which is close to the ferromagnetic transition temperature T_c . For a given chemical composition and oxygen stoichiometry the values of T_p , T_c , and ρ depend on the physical state of the sample. This is particularly true for thin films. For instance, films of the same CMR material grown epitaxially on different substrates can have very different ρ , T_p , and T_c and, consequently, magnetoresistance (MR). It has been proposed that the presence of biaxial strain ϵ_{bi} stabilizes the Jahn-Teller distortion around the Mn^{3+} ions and reduces T_p and increases ρ .³ The effect of ϵ_{bi} is expected to be important in thin films of manganites. Recent experiments have established this.⁴ However, strain is not the only factor. In thin films of CMR materials it is likely that the strain and microstructure together determine the nature of the charge transport. While techniques like x-ray diffraction (XRD), which measure lattice constants averaged over a large length scale and can characterize the strain as “uniform,” however, in mesoscopic or submicron length scales the strain can be inhomogeneous. The film will also contain internal boundaries, discontinuities, and steps. It is therefore expected that the electrical conduction in these materials will be inhomogeneous on submicron length scales. As a result an average parameter like ϵ_{bi} is not enough to describe the current transport in these films. In this paper we address specifically these issues. By using a combination of macroscopic and nanoscopic techniques, we can identify that the inhomogeneities seen in the current path depend on the strain in the film.

(001)-oriented $\text{La}_{0.7}\text{Ca}_{0.3}\text{MnO}_3$ (LCMO) films were grown using pulsed laser deposition (PLD) on SrTiO_3 (STO) and NdGaO_3 (NGO) substrates.⁵ Three types of films were studied: namely, 50-nm-thick film grown on STO [LCMO/STO(50)], 200-nm-thick film grown on STO [LCMO/STO(200)] and 50-nm-thick film grown on NGO [LCMO/NGO(50)]. In Table I, we give some of the relevant details of the samples used. We have made simultaneous measurement

of the topography as well as the local potential in current carrying films using scanning tunneling microscopy (STM) and scanning tunneling potentiometry (STP) (Ref. 6) and correlated them with ρ . Simultaneous STM and STP images were obtained by a double-feedback technique in a home-made STM using Pt-Rh (13%) tips at room temperature and ambient pressure.⁷ For a film with a dc bias applied across its length, a change in the tunnel current can arise from topographic features as well as from a change due to a potential variation across the film. These two contributions are decoupled by using a dc bias for the current in the film and an ac bias for the tunnel junction and two separate feedback loops to regulate the topography and potential. An ac bias is applied between the tip and sample, and the ac tunnel current rectified by a lock-in amplifier is used to scan the tip at a constant current value above the sample, giving the topographic image. Here dc bias is applied across the length of the film in such way that the dc potential at the site of the tip is nulled by the feedback loop. Small changes in the local potential from site to site on the film is thus measured from the feedback voltage of the second feedback loop. Topographic images of all three films were obtained with an ac bias of $V_{pp}=0.05$ V and tunnel current $I_{pp}=0.5$ nA. The potentiometric images of films were obtained with a dc bias. The direction of the current in the film and the fast scan direction (X axis) are kept at an angle of (110°) to avoid any experimental artifacts that might arise. We also check that in the absence of a current in the film there is no STP image.

In Fig. 1, we show the STM images of the three films along with the XRD pattern in the vicinity of the (002) line of LCMO. The LCMO/STO(50) film has an out-of-plane strain $\epsilon_{zz}\approx -1\%$ while the thicker LCMO/STO(200) film has $\epsilon_{zz}\approx -0.03\%$ which is the closest to the limit of resolution of our XRD technique. The 200 nm film is thus fully strain relaxed while the thinner film is strained uniformly. This observation is similar to that seen in LCMO films earlier.⁸ In the LCMO/NGO(50) film the LCMO line was within the NGO peaks and we could place a limit $\epsilon_{zz}\leq 0.02\%$.

TABLE I. Relevant details of the samples used.

Sample name	Substrate	Thickness (nm)	Avg. step-platelet width (nm)	T_p (K)	$\rho_{4.2\text{K}}$ ($\mu\Omega\text{ cm}$)	ρ_p ($m\Omega\text{ cm}$)	E_A (eV)
LCMO/STO(200)	SrTiO ₃	200	35	276	813	57	0.062
LCMO/STO(50)	SrTiO ₃	50	110	215	270	130	0.130
LCMO/STO(50)	NdGaO ₃	50	360	268	216	23.3	0.056

As seen in Fig. 1, the 50 nm films on both the substrates have very clear step and terrace structure that spans over the complete range of image ($\approx 1.5\ \mu\text{m} \times 1.5\ \mu\text{m}$). The same features are seen in atomic force microscopy (AFM) images also, which allow a larger scan range ($\approx 5\ \mu\text{m} \times 5\ \mu\text{m}$). Such a clear step growth mode is rarely seen in manganese films. The presence of clean terraces allow us to do STP in regions which are away from steps or grain boundaries. The terraces themselves are smooth while the steps have a height of $\approx 0.4\ \text{nm}$ which is same as the out-of-plane lattice constant of $0.39\ \text{nm}$. These terraces follow the terraces that are present in the underlying substrates which form when the substrate is heated during the deposition.⁹ In contrast to the 50 nm films, the 200 nm film has an island structure (which we call platelet). The platelets have an average diameter of $\approx 35\ \text{nm}$. These platelets themselves are smooth but the boundary between them shows height variations which are typically a few multiples of $0.4\ \text{nm}$. The roughness seen in the strain relaxed films thus arises from the boundary between the platelets.

A careful analysis of the topography shows an interesting fine structure. Within a terrace or a platelet there is a shallow modulation of the height lasting over distance scales much larger than the lattice spacing. However, the amplitude of the height modulation is a small fraction of the film thickness. This type of shallow height modulation can arise if the strain is not uniform. In LCMO/STO(50) film the mean period of the modulation is $\approx 80\ \text{nm}$ and the rms height modulation is $\approx 0.12\ \text{nm}$ while in LCMO/NGO(50) film the corresponding numbers are $\approx 170\ \text{nm}$ and $\approx 0.03\ \text{nm}$, which is close to our noise-limited resolution. In LCMO/STO(200) the modulation has a period of $\approx 14\ \text{nm}$ and a rms height modulation of $\approx 0.05\ \text{nm}$. In the LCMO/STO(50) film, which is more strained, the rms modulation is the largest, while in the two films with negligible ϵ_{zz} the height modulation is close to the limit of our instrument resolution. We will see below that such a modulation has a close link with the potential drops seen within these terraces.

In Fig. 2 we show the ρ vs T of the three films in a semilogarithmic plot measured down to $4.2\ \text{K}$ by the stan-

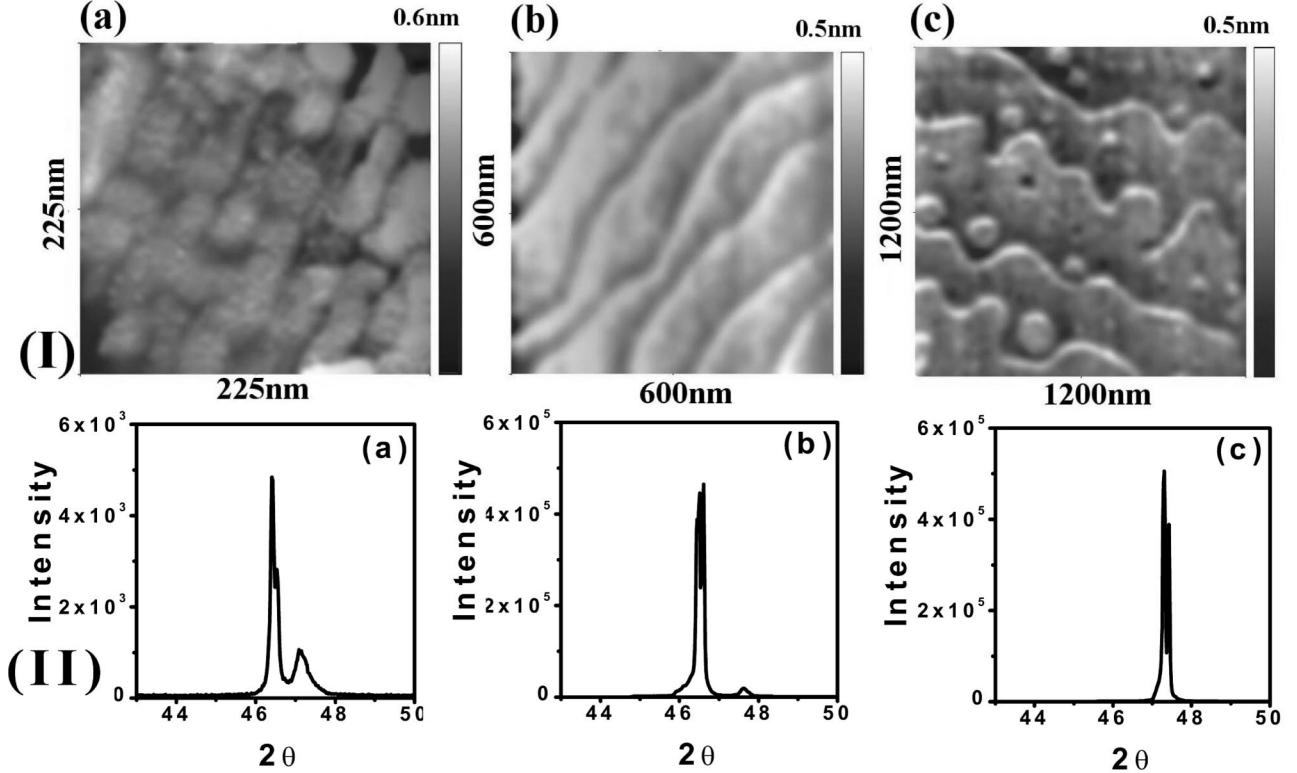


FIG. 1. (I) Topography (STM image) of (a) LCMO/STO(200), (b) LCMO/STO(50), and (c) LCMO/NGO(50), (II) x-ray diffraction pattern around (002) line of (a) LCMO/STO(200), (b) LCMO/STO(50), and (c) LCMO/NGO(50) film.

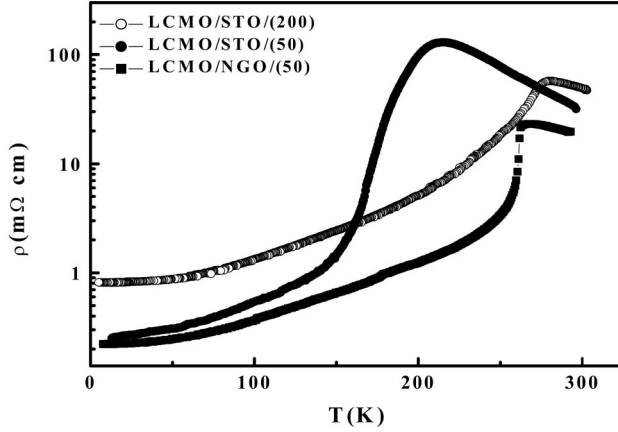


FIG. 2. Temperature dependence of the resistivity of LCMO/STO(200), LCMO/STO(50), and LCMO/NGO(50).

standard four-probe technique. The two 50 nm films have comparable $\rho_{4.2\text{K}}$ although the ρ differ widely at higher temperatures. The 200 nm film has much higher $\rho_{4.2\text{K}}$, although for $T \geq 175\text{ K}$ the LCMO/STO(200) film has much less ρ compared to LCMO/STO(50). Both films on STO have a broad transition with the fully strained LCMO/STO(50) having the broadest transition. The LCMO/STO(50) film, being strained ($\epsilon_{zz} \approx -1\%$), has a severely depressed T_p and high ρ_p . The LCMO/NGO(50) film which has the best lattice match has a single-crystal-like transition with the resistivity falling by a factor of 2 within 7 K of T_p . A good measure of the sharpness of the transition is the derivative $d \ln \rho / d \ln T$ which reaches a maximum at a temperature $T < T_p$. For the film on NGO this has a very high value of 160 while for the films on STO it is $\approx 15-25$.

The effect of strain can also be seen in the temperature dependence of resistivities of the films above T_p . All films have an activated transport for $T > T_p$ with $\rho = \rho_0 e^{E_A/k_B T}$. The activation energies E_A for LCMO/NGO(50) and LCMO/STO(200) with negligible ϵ_{zz} are $\approx 0.056\text{ eV}$ and $\approx 0.062\text{ eV}$, respectively, while that for the strained LCMO/STO(50) is higher ($E_A \approx 0.13\text{ eV}$).

The suppression of T_p with the biaxial strain on ρ is expressed through the relation³

$$\frac{T_p}{T_p^B} = (1 - \Delta \epsilon_{bi}^2), \quad (1)$$

where T_p^B is the T_p of the bulk and Δ is the coupling coefficient with the strain. The value of the biaxial strain $\epsilon_{bi} \approx (3/4)\epsilon_{zz}$ to ϵ_{zz} , which depends on ν , the Poisson ratio which lies typically between 1/2 and 1/3. Using the data for the strained LCMO/STO(50) film we estimate $\Delta \approx 10^4$ which agrees with the theoretical estimates as well as with experimental observations made on $\text{La}_{2/3}\text{Ba}_{1/3}\text{MnO}_3$ films.⁴

The above discussion shows the how average strain in the film (or its relaxation) as seen by such bulk techniques as XRD can affect the transport in these films. In next part we show how the strain or its absence affects the inhomogeneities in transport seen in these films. The inhomogeneity is

seen though the STP data taken at room temperature which is higher than the T_p of the films and thus it is in the paramagnetic phase of the materials where the resistivity is still activated. Past STP studies of CMR films¹⁰⁻¹² on $\text{La}_{0.7}\text{Sr}_{0.3}\text{MnO}_3$ (LSMO) films ($T_c > 300\text{ K}$) were done in the ferromagnetic metallic phase.

Figure 3 shows the STP data which had been taken along with STM data. A clear correlation can be found between the STM and STP data. In all films there are relatively large potential changes near the steps and platelet boundaries. Such large changes in potential indicate that these features may be charged. These jumps are much larger than the average potential drop which arises due to the applied bias. We exercise a note of caution. The experiments were done in ambient, and adsorbates at the steps can lead to charging. However, since the films are conducting, one would expect a substantial screening effect. We believe such a phenomenon does not affect the conclusions reached here. Due to the clean growth patterns in our films, we could get very good STP images. The potential jumps at the steps do not occur abruptly but take place over a length scale which is smaller than the widths of terraces or platelets. The average potential drops in the steps or platelet boundaries vary over a range of $\approx 12\text{ nm}$ for LCMO/STO(200), $\approx 50\text{ nm}$ for LCMO/STO(50), and $\approx 100\text{ nm}$ for LCMO/NGO(50). Such a long-range variation in the potential around a topographic feature can arise from strain variation around such steps which can have a long-range strain field. However, we cannot reach any firm conclusion on these issues from the present data set.

There are two distinct features of the STP data: one occurring at the platelet boundaries and at the steps and the other within a terrace. Often the potential jumps at the platelet boundaries and steps are much larger than the potential variations within the platelets and flat terraces. However, the clear step-terrace pattern in the topography allows us to measure the potential variation within a flat terrace. We find that the potential jumps at the steps have a clear dependence on the nature of strain in the films. In both 50 nm films the step heights are the same ($\approx 0.4\text{ nm}$). However, in the strained LCMO/STO(50) film the potential jumps at the steps are higher than that seen in LCMO/NGO(50). This shows that strain also affects the transport through structures such as the steps in the film.

The strain seems to play a role also in the potential drop seen within the terraces. In all films the potential within a terrace or a platelet shows a uniform drop of the potential and there are fluctuations around that. This uniform potential drop is nearly the same as the average applied potential drop. However, the fluctuations around these potential drops seem to depend on the strain in the film as can be seen in Fig. 3. For instance, in the film LCMO/NGO(50) it is the least and in the strained film LCMO/STO(50) it is 3 times higher and in the strain-relaxed LCMO/STO(200) film it is close to that seen in LCMO/NGO(50) although somewhat higher. There is also a nice correlation of this local potential fluctuation with the shallow height modulation seen in the STM topography. In the LCMO/STO(50) film the height modulation was the highest ($\approx 0.12\text{ nm}$) and in the LCMO/NGO(50) it is the lowest ($\approx 0.03\text{ nm}$). Given the sensitivity of the elec-

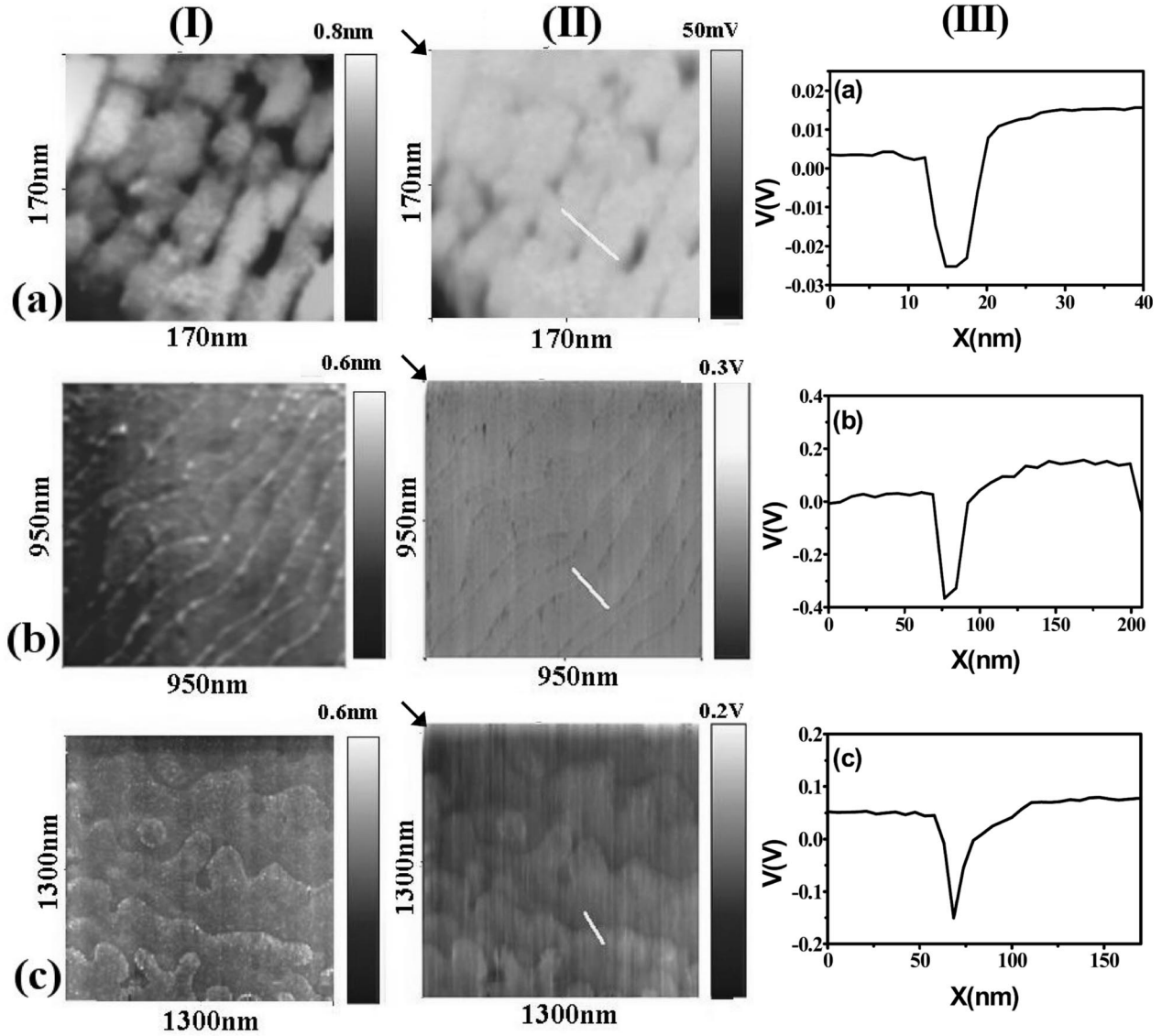


FIG. 3. (I) STM, (II) STP images (III) line scans of STP images across the platelet and step for (a) LCMO/STO(200), (b) LCMO/STO(50), and (c) LCMO/NGO(50) films (arrows shown in the STP images indicate the applied current direction).

trical transport on the strain, in CMR thin films we would like to suggest that the shallow height modulation seen in the terraces leads to local strain fluctuations, which in turn lead to local conductivity inhomogeneities that we pick up in the STP measurements as variations in local potentials. The presence of local strain variations in films thus leads to inhomogeneous current flow in these materials even in the paramagnetic state ($T > T_p$).

STP measurements provide us the measure of the local surface potential $\phi(x,y)$ at the site of the tip. A measure of the local field in the surface plane can be obtained from its gradient $\mathbf{E}_{\parallel}(x,y) = -\nabla\phi(x,y)$.⁷ Here \mathbf{E}_{\parallel} is a good measure of the potential drops occurring over a finite length scale. The quiver plots in Fig. 4 show the variation of \mathbf{E}_{\parallel} along the X and Y directions computed numerically from the potentiometric data array. The length of the arrow indicates the magnitude and head points along the direction of the \mathbf{E}_{\parallel} . This map is a good way to visualize the spots where there is a

relatively large drop in potentials occurring over short length scales. The STP data clearly show that the current flow in the nanometer scale is definitely not homogeneous. The steps and boundaries of the platelets do show large \mathbf{E}_{\parallel} as visualized by the dark contrast on them. Interestingly, even on terraces of the films there are some small conglomerations of dark arrows, which is most prominent in the LCMO/STO(50). This is a reflection of the fluctuations in the local potential seen in these films.

From scans over an extensive area we could generate the statistics of variation of the magnitude of \mathbf{E}_{\parallel} . This is shown in Fig. 4. The average value of the magnitude of \mathbf{E}_{\parallel} in LCMO/NGO(50) is the least for a given current density. In LCMO/STO(50) and LCMO/STO(200) films these are, respectively, ≈ 1.4 and 1.9 times larger. The value of $\rho_{300\text{K}}$ scales very closely with the average magnitude of \mathbf{E}_{\parallel} . When averaged vectorially over a larger length scale, \mathbf{E}_{\parallel} reduces to the applied dc field. This happens typically on a length scale

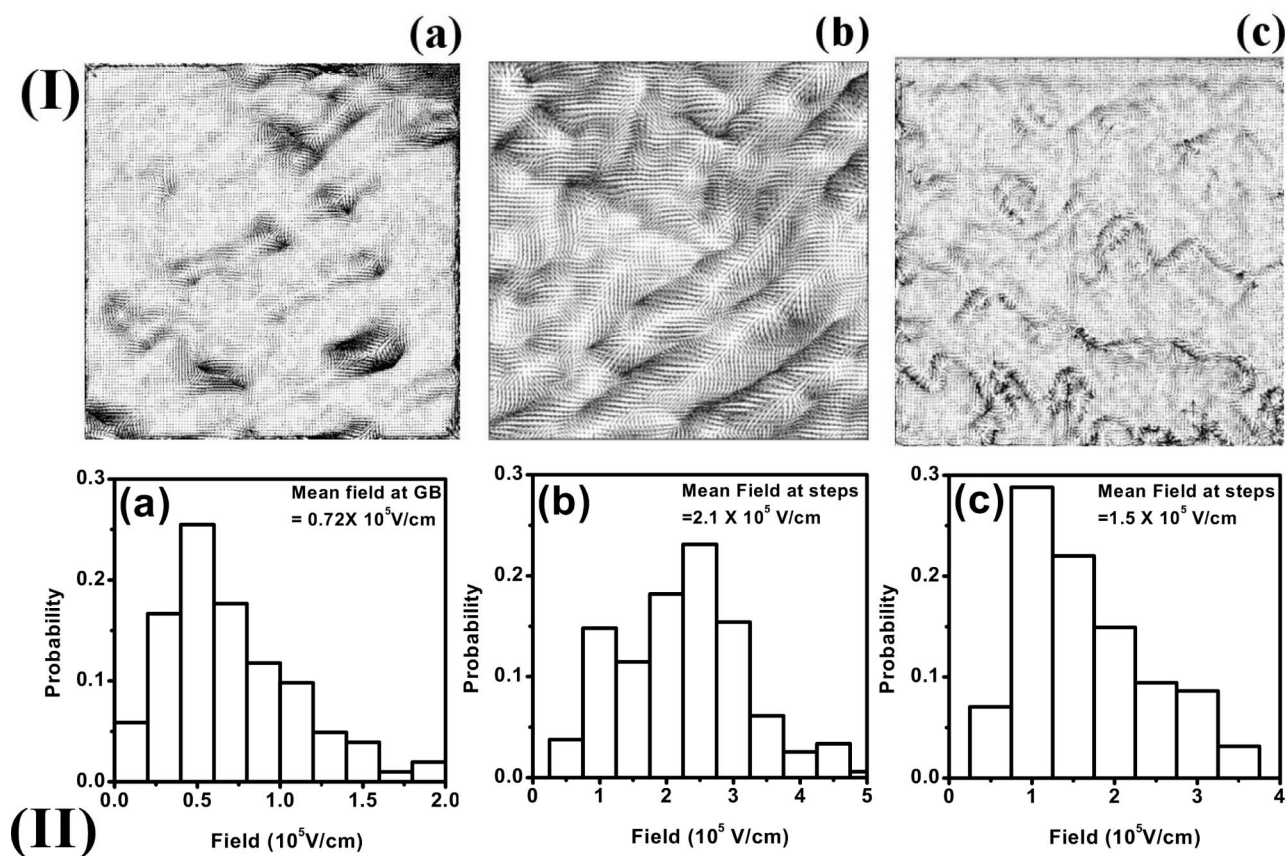


FIG. 4. (I) Quiver plot of the electric field and (II) step and grain boundary field distribution for (a) LCMO/STO(200), (b) LCMO/STO(50), and (c) LCMO/NGO(50).

of ≈ 1000 nm in the thin films which is around 3–10 step widths. From these data one interesting point emerges. It appears that even in some of the epitaxial films, which show single-crystal-type transport behavior like the LCMO/NGO (50) film, a good part of the potential drop occurs at the steps. The transport in manganite films is affected by the large experimental parameter space, spanned by the film thickness, substrate, substrate miscut angle, and surface roughness, which still needs to be explored before definite conclusions can be drawn about the physical relationship between electrical conduction, lattice strain, and possibly also microstructure.

To summarize, we find that the charge transport in manganite films depends on the strain in the film due to

substrate-film lattice mismatch and also on the local strain variations that lead to inhomogeneous current flow. Using STM and STP we were able to identify the role of localized strain in the transport of these films. The correlation of STM topography and STP images shows that local potential fluctuations over smooth terraces and platelets in these films can arise from local fluctuations in strain.

One of us (M.P.) thanks CSIR (Government of India) for support, and A.K.R. thanks DST (Government of India) for a sponsored project under UK-India Technology Fund. Part of this work was funded by the EPSRC of the U.K. and the Royal Society. We thank P.B. Littlewood for helpful discussions.

*Electronic address: mandar@physics.iisc.ernet.in

†Electronic address: arup@physics.iisc.ernet.in

¹*Colossal Magnetoresistance, Charge Ordering and Related Properties and Manganese Oxides*, edited by C.N.R. Rao and B. Raveau (World Scientific, Singapore, 1998).

²*Colossal Magnetoresistive Oxides*, edited by Y. Tokura (Gordon and Breach Science, Singapore, 2000).

³A.J. Millis, T. Darling, and A. Migliori, *J. Appl. Phys.* **83**, 1588 (1998).

⁴Y. Lu, J. Klein, C. Hofener, B. Wiedenhorst, J.B. Philipp, F. Herbristrit, A. Marx, L. Alff, and R. Gross, *Phys. Rev. B* **62**, 15 806 (2000).

⁵M.H. Jo, N.D. Mathur, N.K. Todd, and M.G. Blamire, *Phys. Rev. B* **61**, R14 905 (2000).

⁶P. Muralt and D.W. Pohl, *Appl. Phys. Lett.* **48**, 514 (1986).

⁷G. Ramaswamy and A.K. Raychaudhuri, *Appl. Phys. Lett.* **75**, 1982 (1999).

⁸R.A. Rao, D. Lavric, T.K. Nath, C.B. Eorn, L. Wu, and F. Tsui,

- Appl. Phys. Lett. **73**, 3294 (1998).
- ⁹K. Szot and W. Speier, Phys. Rev. B **60**, 5909 (1999).
- ¹⁰J.J. Versluijs, F. Ott, and J.M.D. Coey, Appl. Phys. Lett. **75**, 1152 (1999).
- ¹¹B. Grevin, I. Maggio-Aprile, A. Bentzen, L. Ranno, A. Llobet, and Ø. Fischer, Phys. Rev. B **62**, 8596 (2000).
- ¹²B. Grevin, I. Maggio-Aprile, A. Bentzen, O. Kuffer, I. Joumard, and Ø. Fischer, Appl. Phys. Lett. **80**, 3979 (2002).